A NOVEL MACROSCOPIC TECHNIQUE TO MEASURE THE NANOMECHANICS OF

DURABLE MULTIFUNCTIONAL NANOSHEETS

A Thesis
Submitted to the Graduate Faculty
of the
North Dakota State University
of Agriculture and Applied Science

By

Abu Md Niamul Taufique

In Partial Fulfillment of the Requirements
for the Degree of
MASTER OF SCIENCE

Major Department:
Physics

April 2017

Fargo, North Dakota

NORTH DAKOTA STATE UNIVERSITY

Graduate School

Title

A NOVEL MACROSCOPIC TECHNIQUE TO MEASURE THE

NANOMECHANICS OF DURABLE MULTIFUNCTIONAL NANOSHEETS

By

Abu Md Niamul Taufique

The supervisory committee certifies that this thesis complies with North Dakota State University's

regulations and meets the accepted standards for the degree of

MASTER OF SCIENCE

SUPERVISORY COMMITTEE:

Erik Hobbie

<small>Chair</small>

Orven Swenson

Mohiuddin Quadir

Sylvio May

Approved:

12 April 2017	Sylvio May
Date	Department Chair

ABSTRACT

In the recent advancement of nanotechnology, carbon nanotubes (CNTs) have shown promise and potential for a wide variety of applications due to their excellent mechanical, electrical, and optical properties. A network of single wall carbon nanotubes (SWCNTs) is of interest due to its potential applications in flexible electronics, composites, constructional materials, and so on. Characterizing the mechanical properties of these thin films will be critical to achieving a full understanding of their behavior, yet relatively few experimental methods exist for querying the deformation mechanics of these films. To provide additional insight into the large-deformation mechanics of these films, we propose a novel method for evaluating the mechanical properties of thin SWCNT films. We provide theoretical background, describe the experimental approach, and use a MATLAB based analysis to extract the film modulus. Finally, we compare our results to existing wrinkling-based measurements, where we find reasonable agreement between the two techniques.

ACKNOWLEDGEMENTS

DEDICATION

This thesis is dedicated to my Mom, Dad, and sister.

TABLE OF CONTENTS

LIST OF FIGURES

1. INTRODUCTION

Thin films and coatings play a very important role in our day to day life, from composite materials to electronics, optics, constructional materials, and so on. Yet devices are getting smaller in size and incorporated with more features, buildings are getting stronger and self healing with the capability of monitoring their own health by incorporating new technologies, resulting in a need to find new materials. Over the past several years, nanotechnology has become an emerging area of research, with nanomaterials being of particular interest. Nanoscale thin films of different materials have gained tremendous interest for applications such as MEMS [10], solar cells [34], lithium ion batteries [7], and so on. Understanding the different physical properties of nanomaterials is important for practical applications. In the case of thin films, durability and rigidity have a significant impact on their usefulness. Yet, few experimental procedures exist in the literature for finding the mechanical properties of nanoscale thin films. For thin films made of polymers, some surface characterization techniques, such as nanoindentation and atomic-force microscopy (AFM), can give us important insight about the polymer chain confinement, and modulus of elasticity, E, as a function of film thicknesses [8][42]. Experiments can also be done to extract information from larger length scales based on direct approaches like polymer-melt bubble formation [26], while other methods like wrinkling give the mechanics of the films over microscopic to macroscopic length scales [35]. However, these more or less represent the existing techniques for measuring the mechanical properties of nanoscale thin films. Therefore, a novel method to extract the macroscopic mechanics of nanostructured thin films would be of great importance, specifically if the materials have strong potential impact for current science and technology fields.

Among the materials highly touted from this perspective, single-wall carbon nanotubes (SWCNTs) keep showing strong potential for applications. Basically, SWCNTs can be considered as a single monolayer graphene sheet rolled up to a hollow cylinder. It is approximately 1 nm in diameter and can be 100 nm to millimeters in length. The monolayer can be rolled up with different molecular symmetry [2], can be either metallic or semiconducting, and can have several potential applications in microelectronics [6]. SWCNTs have a polymer-like shape and a high elastic modulus, although their full potential in mechanical applications remains a topic of research [23].

In our attempts to engineer durable nanotube coatings, our group has worked diligently to measure the mechanics of thin nanotube films deposited on elastic polymer substrates [14][11]. Our group has studied the mechanics of very thin SWCNT networks using the 'wrinkling' method, which was actually developed to find the mechanics of thin polymer films [38][32]. The results provide significant insight into the mechanics of SWCNT thin films, providing glimpses of moduli on the order of hundreds of GPa, but with suggestions of plastic behavior under rather small strains [14]. Out previous results also discuss the modes of mechanical failure under applied deformation, which we suggest is due to bundling of the connected nanotubes through van der Waals (vdW) force [16].

For several potential applications - many of them in 'flexible electronics' - it would be of tremendous importance to provide additional insight into the mechanics of nanotube thin films. In my thesis, I will describe the fundamentals of CNTs in chapter 2. The thin film production method is described in chapter 3. In chapter 4, I will describe the existing techniques to measure the nanomechanics of thin films. Then finally in chapter 5, I will describe the theoretical background, experimental procedures, data extraction, and the results and discussion of our new approach to find the mechanical properties of SWCNT thin films.

2. CARBON NANOTUBES

2.1. History

Carbon nanotubes (CNTs) were discovered by Sumio Lijima [17], where he reported finite, hollow, tube-like, fullerene C_{60} structure. He was using an arc discharge technique, which was similar to the production technique of fullerene [21]. He found the stack of nanotubes at some regions of the electrode. Using a high-resolution transmission electron microscope, he was able to identify the diameters of the coaxial microtubules, and the type of nanotubes were named multi-walled carbon nanotubes (MWCNTs). Later, Lijima synthesized single-shell nanotubes [18] of 1 nm diameter, which were named single-walled carbon nanotubes (SWCNTs). After the discovery of CNTs, tremendous work has been done to study the synthesis, physical properties, and applications within the last two decades.

2.2. Synthesis

Initially CNTs were synthesized at high temperature environment using arc discharge or laser ablation method. In the arc discharge technique, above 1700 °C temperature is usually used. In most of the cases, for synthesizing MWCNTs, DC voltage has been supplied between two graphite electrodes in either vacuum or gaseous medium such as He, NH_3, CH_4, H_2 etc. It has been reported that different gases produce negligible difference in the morphology of CNTs [20]. However, CNT morophology can be controlled more precisely using a composite anode configuration with graphite. SWCNTs can be synthesized using composite anode with various composite materials, such as Pd, Co, Pt, Fe, Ni, etc [27]. Several works have been done to get a mass production of CNTs using pulse laser deposition (PLD) technique, where the morphology of CNTs depend on many factors, such as energy, power, frequency of the pulsed laser, and some other environmental factors of the system.

The laser ablation technique was first introduced by Smalley's group [9], where they used a similar technique to the arc discharge method except that the composite sample (a graphite plate with usually Ni or Co catalyst) was hit by the laser instead of arc [19]. Usually CO_2 and Nd:YAG lasers have been used for CNT synthesis, and it has been observed that with increasing laser power of CO_2 laser, the average diameter of SWCNTs increased [4] [25].

Recently, these two methods have been replaced by chemical vapor deposition (CVD) technique, since CVD can be used to accurately control the alignment, chirality, diameter, length, purity of nanotubes at relatively low temperature (800 °C) [13]. The major advantage of CVD method is that it's easy to control the reaction course and relatively purified CNTs can be produced [43], and so on. Now, either thermal [37] or plasma enhanced (PE), catalytic chemical vapor deposition (CCVD) is the standard method to synthesize CNTs.

However, no matter what method is used, CNTs are always produced with impurities depending on the technique. Major impurities are related to the carbonaceous particles including fullerenes, nanoparticles of carbon, catalysts that are included to the composite graphite electrodes [27]. These impurities modify the expected properties of CNTs, and it is still a challenge to develop an efficient and inexpensive purification method [22].

2.3. Chirality
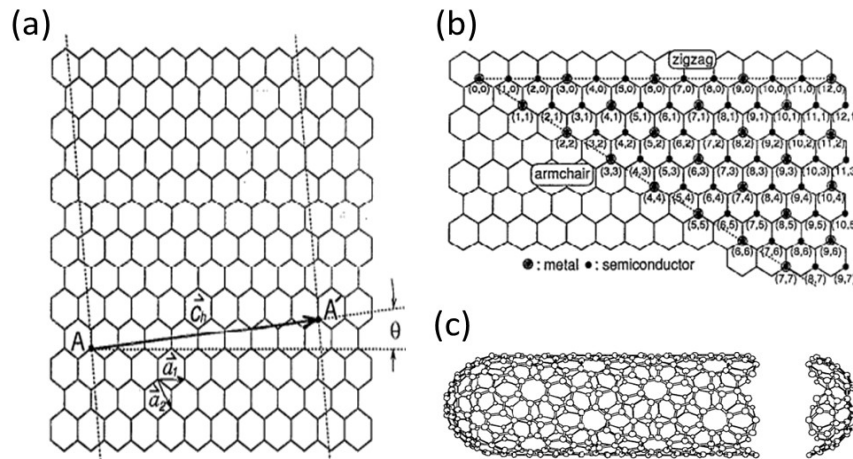
Figure 2.1. (a) A graphene monolayer, where single-walled nanotubes can be made by rolling up the sheet. Nanotube properties can be determined by chiral vector $\vec{C}_h$. Here, θ is the chiral angle and $\vec{a_1}$ and $\vec{a_2}$ are the unit vectors of graphene, (b) possible vectors for metallic and semiconducting SWCNT chiralities, and (c) a chiral nanotube [30].

CNTs can be thought of as a rolled-up sp^2 hybridized graphene sheet, where the electronic properties of CNTs are dictated by the chiral (n,m) vector [31], $\vec{C}_h = n\vec{a_1} + m\vec{a_2}$, where n and m

are integers. These n and m integers define if the CNT is metallic or semiconducting $-$ if $2n + m$ is divisible by 3, the nanotube will be metallic, and any other combination will be semiconducting [30].

3.   CNT FILM PRODUCTION

3.1. Materials

The nanotubes used for this experiment are CoMoCat SG65i SWCNTs.These nanotubes were synthesized by the CoMoCAT^{TM} catalytic chemical vapor deposition technique. In this method, CO is decomposed into C and CO_2 when the temperature in the chamber rises to more than 700°C at 1-10 atm pressure. A Co:Mo catalyst is used to grow the SWCNTs on a silica substrate. In this process, the nanotubes are deposited in the form of a powder, where the carbon composition is approximately 95% with roughly 93% SWCNTs. Among the SWCNTs, roughly 93% of the composition is semiconducting, from which about 40% are (6,5) SWCNTs. The average diameter of the SWCNTs is about 0.76-0.78 nm, with the tube aspect ratios approaching 1000. The SWCNT powder was dispersed at approximately 1 mg SWCNT/mL in an aqueous solution of 2% mass fraction of sodium deoxycholate (DOC) using tip sonication with the tip size being 0.64 cm (Thomas scientific). Sonication is done in ice water at 1 W/mL power for 1 hour. For purification, the suspensions were centrifuged at an acceleration of 21000g for 2 h to remove impurities and bundles.[15] An atomic force microscope (Model 5500, Agilent Technologies) operated in tapping mode was used to measure the length distribution of CNTs. For this, a solution was prepared and refrigerated with 30 μL of aqueous SWCNT and 150 μL of DI water. A silicon wafer was cut into small pieces and these were soaked in the refrigerated solution for 24 hour. Before the final measurement, the silicon chip was soaked in ethanol for 2 hours to remove residual surfactant. The distribution of length (L) had a mean length of 670 nm, and can be described by a log-normal distribution; $\rho(L) = A exp[-\{ln(L/L_0)/\sigma\}^2]$ with $A = 12$, $L_0 = 300$ nm, and $\sigma = 0.62$ nm. The purified colloidal SWCNT suspension is shown in figure 3.1.(a).

3.2. Methodology

To prepare the thin films, a vacuum filtration system (VFS) was used. For this, a cellulose-easter filter-paper of 0.5 μm was soaked in a 5% solution of ethanol to remove dust particles. The filter paper is shown in figure in figure 3.1.(b). DI water was used to prepare all the solutions. A 10% aqueous ethanol solution was prepared using 200 mL of DI water and 20 mL of ethanol. A reservoir beaker with an outlet pipe was used. A stopper was placed on top of the reservoir beaker.

A bubble level was used to level the stopper because without leveling, a gradient on the film can be produced. The filter paper was then placed on the stopper. Another beaker with a petri-dish on top was placed on the stopper, where the petri-dish was used to keep the dust out of the solution. Then, the stopper was re-leveled again. After leveling, the 220 mL of 10% ethanol solution was poured into the top beaker.
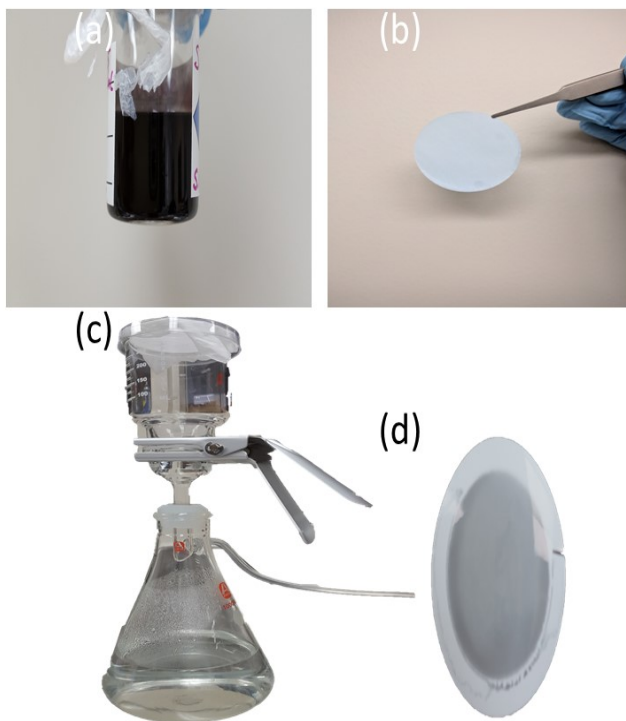
Figure 3.1. Film production, (a) the purified nanotube solution, (b) cellulose-easter filter paper before adding the SWCNT solution, (c) the experimental setup, (d) filter paper supported nanotube thin film.

The total experimental set up is shown in figure 3.1.(c). It was kept untouched for approximately 10-15 minutes to stabilize the solution. In the mean time, the volume of SWCNT solution was calculated to make a film of the desired thickness. For example, 7.2 μL of AP CNT and 496.4 μL DI water was used to produce a film of approximately 20 nm thickness. To prepare this solution, the aformentioned amounts of AP CNT and DI water were mixed in a vial. The solution was then taken using a volumetric pipette, which was gently expelled above the filter paper into the 20 % ethanol solution. In order to produce a film with a minimum gradient, the CNT solution was

deposited as a broad uniform droplet in the center of the filter and the solution was left undisturbed for 10-15 min. A vacuum was then applied until all of the ethanol solution had passed through the filter paper. When the surface of the deposited film was dry, the top beaker was removed, and the filter paper was kept on the topper for 20-30 minutes. Finally, the filter paper was taken out from the topper, to be cut into pieces and used for further experiments. A filter-paper supported thin SWCNT film is shown in figure 3.1.(d).

4. MECHANICAL PROPERTIES OF THIN FILMS

There are a few methods in the literature which can be utilized to measure the mechanical properties of nanoscale thin films. Most of these methods have some advantages and disadvantages, which are explained in this chapter.

4.1. Nanoindentation

To find the modulus of any sample using nanoindentation, a tip of known modulus is used. Typically diamond tips are used for nanoindentation. Qi et. el. [28] used a diamond-tip based nanoindentor to indent a vertically aligned nanotube forest and find the bending modulus of individual nanotubes. They operated the atomic force microscope in a consecutive contact mode and found the modulus of individual multiwalled carbon nanotubes. As another example, the mechanical characterization of a multilayer SWCNT film was done by Wei et. el. [41]. They used self-assembled SWCNT films deposited on a silicon substrate. They prepared a PDDA/SWNT bilayer and stack 40 of them on the substrate. Then they used a commercially available nanoindenter to find the loading and unloading characteristics of the thin film. Finally, they found the modulus of the bilayer using the conventional Young's modulus calculation technique associated with nanoindentation. In this technique, they limit the penetration depth to minimize substrate effects.

However, several papers have been published expressing the opinion that indentation-based measurements of elastic modulus might be influenced by the substrate [40][29][3][24][5]. Also, both AFM based and commercially available nanoindentation measurements require expensive instrumentation.

4.2. Wrinkling

This method provides an conceptually simple and accessible platform for studying the mechanical behavior of nanoscale thin films.

In this method, the filter-supported SWCNT film was first prepared using exactly the same procedure discussed previously. Then the SWCNT nanomembrane was deposited on a polydimethylsiloxane (PDMS) substrate by placing it face down on prestretched PDMS and dissolving the filter paper with acetone. Releasing the prestrain in the PDMS substrate produced the wrinkling
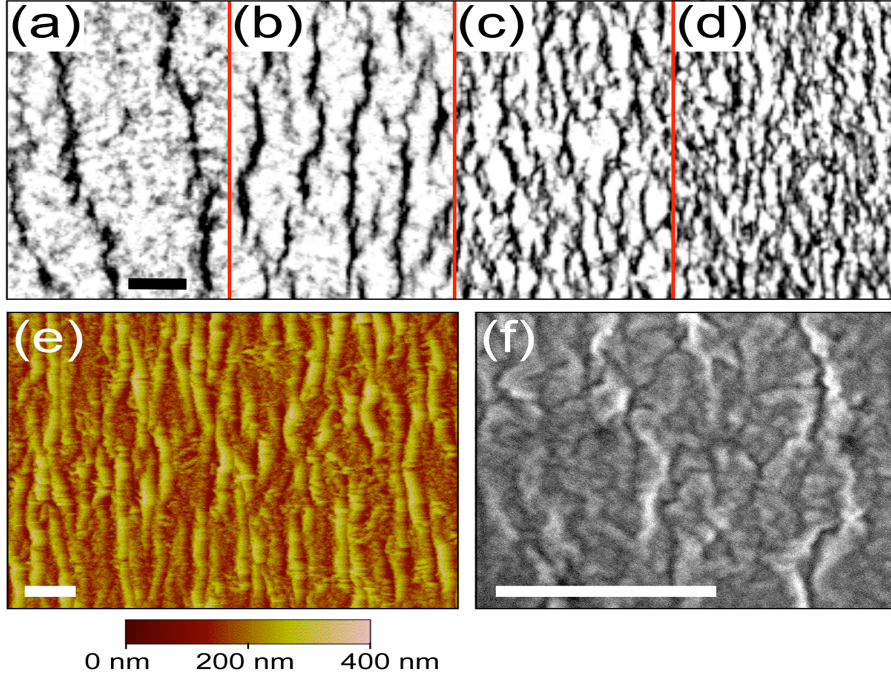
Figure 4.1. Optical micrographs of different wrinkling patterns for a thin film (surface mass density of SWCNTs = 3.5 $\mu g/cm^{-2}$, $L = 130nm$), (a) at 2.5% strain, (b) at 5% strain, (c) at 10% strain, (d) at 20% strain, (d) AFM, and (e) SEM images of the topography at 5% strain. (all the scale bars are 5 μm) [14]

patterns shown in the figure 4.2. By fitting the strain response to a simple power-law expression, the zero-strain behavior was extracted as $E_f(0) = (h/h_c - 1)^\beta$, where h_c is the percolation threshold and $\beta \approx 1$ [12]. However, in the case of SWCNT films, this technique also implies porosity and inhomogeneity, which might affect the interpretation of the wrinkles by triggering localization, ridge formation, and length-scale bifurcation [33].

5. A NOVEL MACROSCOPIC TECHNIQUE TO MEASURE THE NANOMECHANICS OF DURABLE MULTIFUNCTIONAL NANOSHEETS

In this chapter, I will describe the theoretical background, experimental design, and results. Our research is mainly focused on developing an entirely new technique to measure the nanomechanics of SWCNT thin films. In our experiment, the idea was to manipulate the film, using a magnet, away from its equilibrium position and capture the free movement back to equilibrium to determine its relaxation time and eventually find the Young's modulus of the film. First, I used 'Image J' software to process the captured video and make it a binary image string. For further processing, I created a MATLAB code to analyze those images to find the X-Y coordinates of each pixel and arrange them into vectors. Then using MATLAB, I manipulated those vectors to calculate the curvature distribution along the contour of the film. Using that data, I found the relaxation time, which can be used to find the modulus of the film. To find the film thickness, I used a combination of AFM and optical extinction spectroscopy.

5.1. Theoretical background

If a sheet is bent, a certain amount of elastic energy is stored in the sheet. If the bending force is then removed, the sheet will start moving back towards its initial position and the energy will be dissipated into the surrounding medium.

To model this relaxation process, we first consider a linear model of elastic recovery. For simplicity, we assume that the sheet bending is symmetrical around the z axis, where z is the local displacement from equilibrium, as shown in Figure 5.1. We also consider that the force as a function of local curvature – κ, formed on the z axis around the deformation size l – is symmetric. The sheet displacement z can be represented as a parabolic function of the deformation size l, where the vertex goes through the origin, which implies

$$z(l) = al^2 \tag{5.1}$$

11
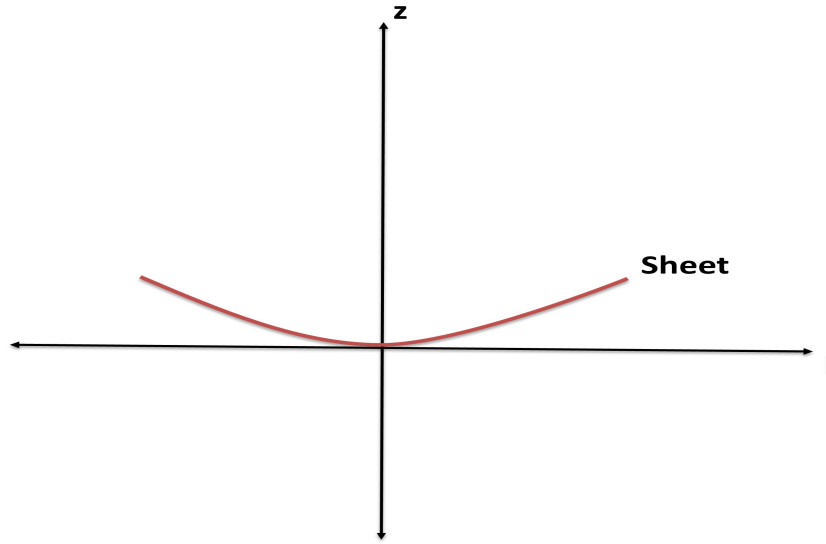
Figure 5.1. Bending of a sheet to a parabolic structure, where z represents the local displacement away from the equilibrium position and l represents the deformation size.

$$\frac{d^2 z(l)}{dl^2} = 2a$$

According to the definition of curvature

$$\frac{d^2 z(0)}{dl^2} = 2a = \kappa$$

From (5.1), we get

$$z = \frac{\kappa l^2}{2} \tag{5.2}$$

Consider a sheet of length L, thickness h, and width w, where within the deformation region l, $h << w$. If the deformation area is A_0 and the deformed area of the sheet is A, we can write

$$A = A_0(1 + \kappa z) \tag{5.3}$$

If the Young's modulus of the sheet is E, then the energy density, u, of one layer of the sheet due to bending can be written as

$$u = \frac{E}{2} \left(\frac{A - A_0}{A_0} \right)^2 \tag{5.4}$$

12

So, the total energy of the sheet, U, is

$$U = A_0 \int_{-h/2}^{h/2} u \, dx.$$

$$U = A_0 \int_{-h/2}^{h/2} \frac{E}{2} \left(\frac{A - A_0}{A_0} \right)^2 dx.$$

Using (5.3)

$$U = \frac{wlE}{2} \int_{-h/2}^{h/2} \kappa^2 z^2 \, dx.$$

$$U = \frac{wlE\kappa^2 h^3}{24}$$

Writing κ in terms of z from (5.2),

$$U = \frac{wEz^2 h^3}{6l^3}. \tag{5.5}$$

This is the sheet energy, which will be dissipated due to friction between the fluid and the nanosheet. This dissipation can be approximated by the Rayleigh dissipation function, R. For a fluid of dynamic viscosity μ and a length scale associated with the hydrodynamic response, l_0, we can approximate the Stokes' drag as

$$F_d = B\mu l_0 \dot{z} \tag{5.6}$$

where $\dot{z}$ is the velocity of the object with respect to the fluid and B is a dimensionless scaling factor. This force can be written as the negative of the velocity gradient of the Rayleigh dissipation function, from which it can be derived that

$$R = -\frac{B\mu l_0 \dot{z}^2}{2} \tag{5.7}$$

Using (5.5) (5.7) in the over-damped limit, the force balance equation can be written as

$$\frac{\partial U}{\partial z} = \frac{\partial R}{\partial \dot{z}} \tag{5.8}$$

$$B\mu l_0 \dot{z} + \frac{wEh^3 z}{3l^3} = 0 \tag{5.9}$$

13

The same equation can be written for κ, where the solution is

$$\kappa = \kappa_0 exp(-t/\tau) \tag{5.10}$$

and where τ is the characteristics relaxation time of the sheet given by

$$\tau = \frac{3\mu l_0 l^3}{wEh^3} \tag{5.11}$$

Here, B is considered to be on the order of 1 for the simplicity of our calculation.

5.2. Sample preparation

The first step to prepare free standing thin film was to cut the filter-paper-supported nanosheet into four ribbon-like pieces. Then it was cut into several rectangular pieces of various lengths and widths using a scissors and a tweezers. One end of the film was then held with inverted tweezers and the other end was 'doped' with a very dilute concentration of 1 micrometer super-paramagnetic PS colloids (Polysciences). Before use, the colloidal suspension was sonicated with a 3510, Branson model sonicator, shown in figure 5.2.(a).
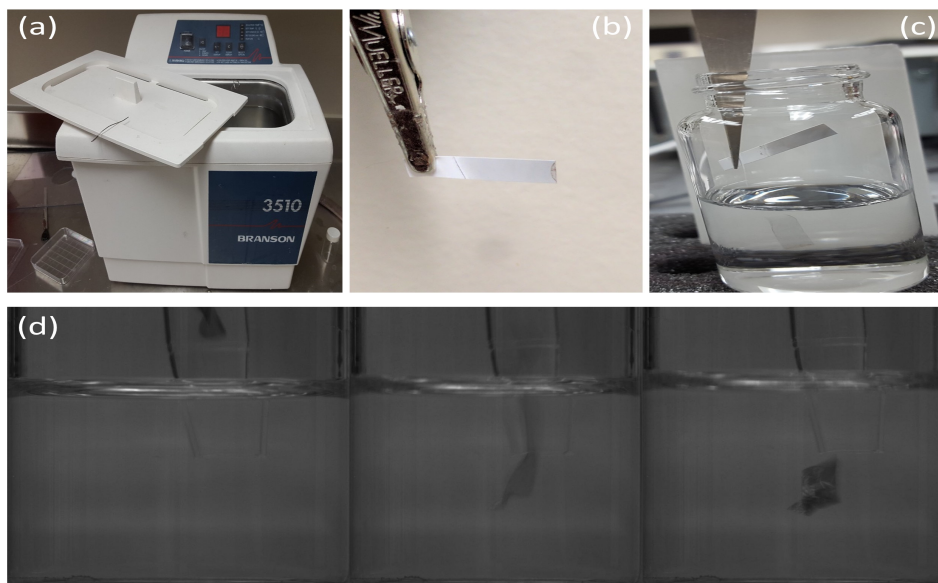

Figure 5.2. (a) Sonicator used for the sonication of the magnetic particles, (b) a rectangular filter-paper-supported thin film doped with magnetic particles at one end, (c) dropping the flag with the help of tweezers into the Acetone, and (d) pipette mediated handling and transfer of the thin film.

For doping, a very small amount of material was used to keep the dopant level as low as possible, and it was uniformly distributed along the width of one end of the film. Upon drying, these particles diffuse into the nanotube network and stick to the network due to van der Waals (vdW) attraction. The doped filter-paper supported film is shown in figure 5.2.(b). The 'doped' end of the nanotube film acts as a handle to manipulate the film with an external magnetic field. The next step was to get rid of the filter paper to produce a free standing nanofilm. For this, a vile half full of acetone was taken and kept untouched with no cap on it to stabilize the fluid, which is important because waves in the fluid can tear up the film, as the film is vulnerable at the very beginning. The dropping procedure in the acetone vile is shown in figure 5.2.(c).

After soaking the film in acetone for about 30 minutes, the film was transferred to a second vile half full of acetone using a volumetric pipette and kept in acetone for at least 12 hours. Then, the film was transferred to the third vile half full of acetone and kept approximately 30 minutes. These successive baths are critical because they eliminates the residue of the dissolved filter paper. To get rid of as much residual surfactant (DOC) as possible, three successive baths in ethanol were performed. For this, a pipette was again used to transfer the film from acetone to the first vile of ethanol, where the film was kept for about 30 minutes. Again, the film was transferred to the second vile half full of ethanol and was kept there for approximately 12 hours. A third bath was done by transferring the film to a third vile half full of ethanol where it was kept for about 30 minutes. These successive baths in acetone and ethanol make the film suitable for further experiments. The pipette-mediated transfer procedure is shown in figure 5.2.(a).

5.3. Methodology

To find the modulus of the film, the first step was to find the relaxation time of the film. For this, we first transferred the film from the glass vile to the quartz cuvette filled with ethanol. A scale bar was attached to the cuvette to get the proper length-scale calibration of the film, as shown in figure 5.3.(a). The presence of fluid in the cuvette is essential because it screens the vdW attraction forces and prevents the film from irreversible folding under large deformation. Then, a bubble with approximately 2 mm diameter was carefully created in the cuvette. However, the bubble size was not the same for every film, it was measured when the video was analyzed. After the bubble creation, the film was attached to the bubble on the bottom of the cuvette as shown in figure 5.4.(a). The film was trapped such that the magnetic side of the film was free to move. The cuvette
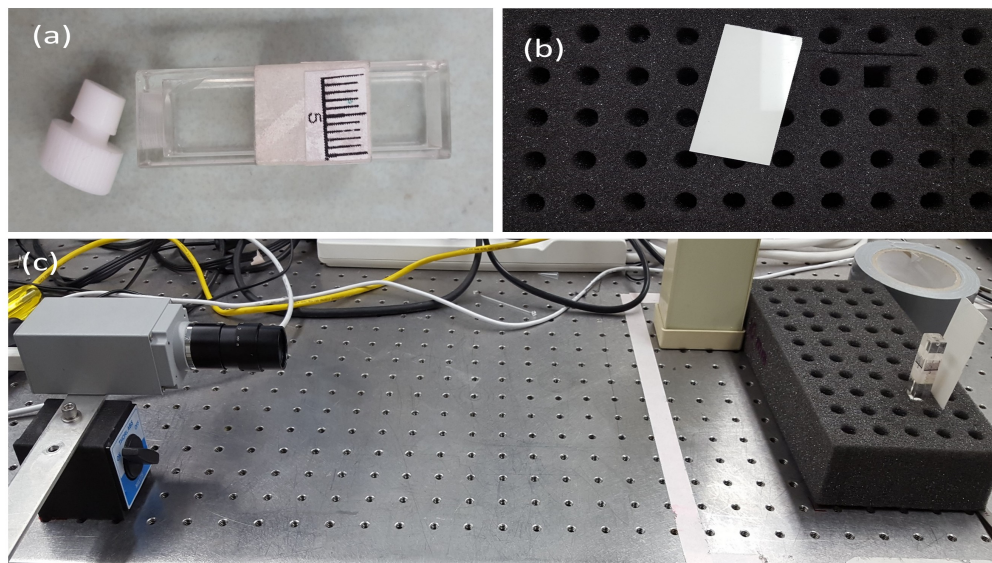
Figure 5.3. (a) The quartz cuvette with a scale bar mounted on it, (b) the drilled sponge cuvette holder and the white polished background, and (c) the complete experimental set up.

was then held by a sponge support as shown in figure 5.3.(b). To eliminate the background during digital video acquisition, a sheet of 37 mm width polished with white paint was placed behind the cuvette. A camera was used to capture the digital video at 17 frames per second. A machine vision software, 'Capture OEM' from PixeLINK, was used to capture the video. The complete experimental setup is shown in figure 5.3.(c). The bubble-attached film was kept untouched for 30 minutes to avoid the residual flow of ethanol within the cuvette. In the mean time the camera was placed and the computer was set up to take the digital video. Then a magnet with sufficient strength was placed near the cuvette close to the magnetic end of the film, which made the film disengage from the top of the cuvette as shown in figure 5.4.(b). Subsequently, the magnet was placed on the other side of the cuvette and the film was dragged to its final deformation state. However, careful handling was done to make sure that the film was not stuck to the bubble at the point where maximum curvature was created in the film. The film was then was kept at the same stage for approximately 2-3 minutes to avoid the residual flow created by any movement of the film and to allow hydrodymanic transients associated with prior film handling to decay. Finally, the magnet was removed and the movement of the film was captured by the camera. Six different positions of a 35 s video are shown in figure 5.4.(c).

16
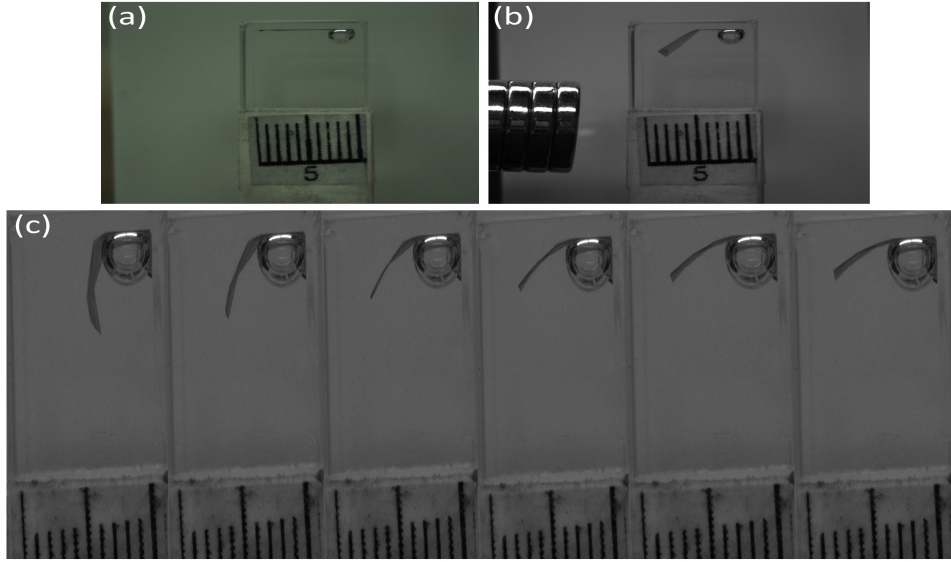
Figure 5.4. (a) A bubble-trapped thin film at the top of the cuvette, where the magnetic end is away from the bubble. (b) Initial deflection of the film using the magnet, (c) final deformation state of the film at the time of removing the magnet (left) and the movement of the film after 7s (from left to right), where the last frame on the right represents the final position of the film.

5.4. Result and Discussion

To demonstrate the analyzing procedure, a 52 nm film was used.

5.4.1. Relaxation time measurement

Initially, the video was converted to a binary video of 600 frames using the 'Image J' software. The binary image of the final image of deformation is shown in figure 5.5.(a) and the extracted contour based on MATLAB is shown in figure 5.5.(b). The final relaxation state after 35 s is shown in figure 5.5.(c), where the extracted contour is shown in figure 5.5.(d).

A MATLAB algorithm was developed to analyze the local curvature distribution $\kappa = |d^2\mathbf{r}/ds^2|$ along the contour length s, where $\mathbf{r}$ is the position vector which locates an element along the contour length. The curvature distribution is shown in figure 5.5.(e) for the contour length innterval from 2 mm to 4 mm, for the six different film positions shown in figure 5.4.(c), where the inset shows the local point of interest. Finally, the change in the maximum curvature along the contour length of the film with time is shown in figure 5.5.(f) using a false color plot. An exponential relaxation, $\kappa = \kappa_0 exp(-t/\tau)$, was fit to the data, where $\tau = 3\mu l_0 l^3/wEh^3$ is the characteristic relaxation time of the sheet. The fit is shown in figure 5.5.(g).
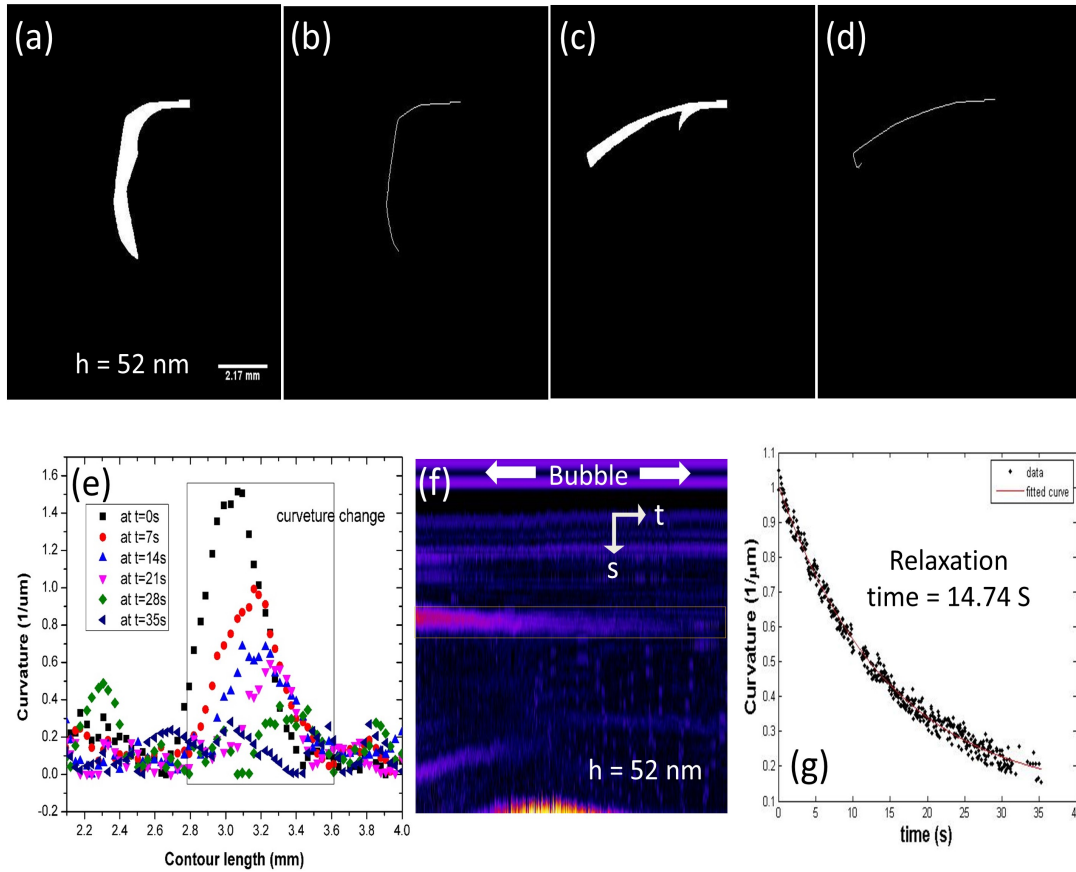
Figure 5.5. (a) An 'Image J' processed binary image of the final position of the film, (b) the region of interest extracted from (a) using MATLAB with the same scale as (a), (c) final position of the film after relaxation [same scale as (a)], (d) extracted region of interest [same scale as (a)], (e) curvature vs. contour length of the region of interest for six different positions of the film shown in figure 5.4.(c), (f) the false color curvature plot of the contour length vs. time of the total film relaxation where the bright color represents the highest curvature, (g) the exponential relaxation of the film with a MATLAB based exponential fitting.

5.4.2. Thickness measurement

After finding the relaxation time, the next step is to find the thickness of the film. To do that, the film was deposited on a glass substrate using the pipette mediated transfer method. Special care was taken to deposit the film such that the film did not break and there were no wrinkles or folds.

In figure 5.6.(a), nine films of different thicknesses deposited on a glass substrate are shown, where figure 5.6.(b) demonstrates a closer view of the glass-film interface. Magnetic particles adhered to a film are shown in figure 5.6.(c). To find the thickness, our first step was to find the

18
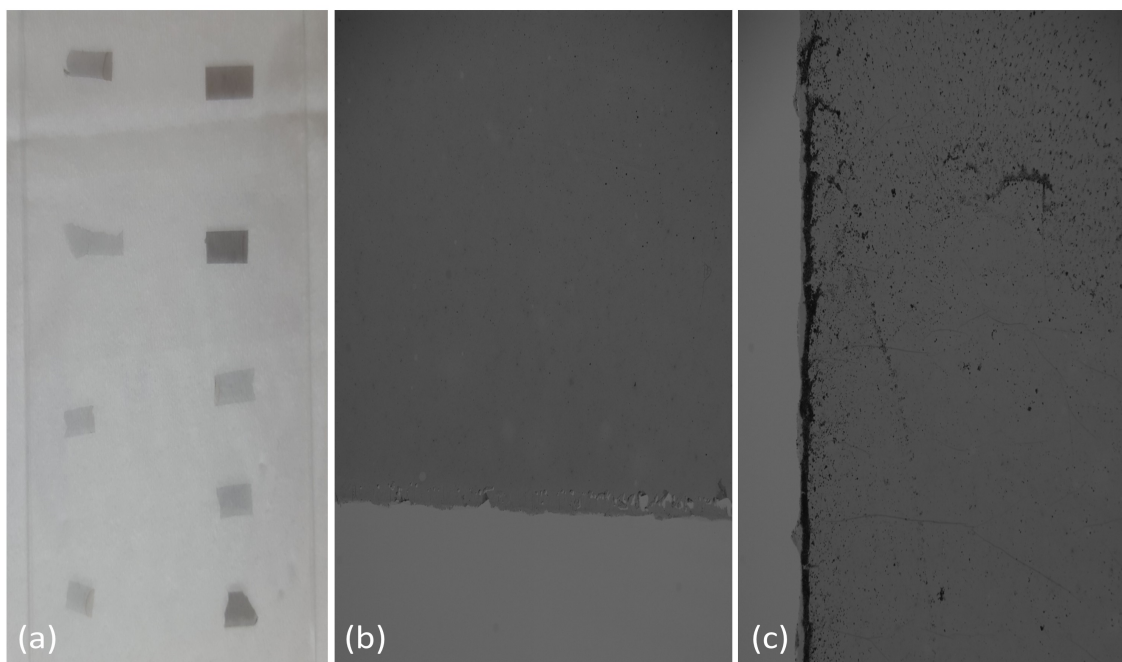
Figure 5.6. (a) Several films of different thicknesses were deposited on a glass substrate. (b) A zoomed-in view of a film deposited on glass. (c) A zoomed in image of the magnetic particles attached to the film, where the size of the particles are 1-2 μm.

extinction coefficient of the film. The optical extinction of the film was measured in transmission using a highly stable broadband lamp for excitation and a spectrometer (Ocean Optics QE65000) for the detection, as shown in figure 5.7.(a). The second order absorption peak of the CoMoCat SWCNTs was found near 583 nm, where an example of the spectral data is shown in figure 5.7.(b). The data was taken for a series of films. For each film, three or more measurements were taken to get the average. The same films were taken to the AFM to measure the thickness, measuring the step height. Careful measurements were done such that AFM measured the same spot probed in the optical measurements. An AFM image is shown in figure 5.7.(c), where figure 5.7.(d) depicts a step height (thickness) of approximately 52 nm. Finally, using the Beer-Lambert law, $I(h) = I_0 exp(-\alpha h)$ where h is the known thickness of the films, the AFM calibrated data give us the extinction coefficient α of the films near 583 nm, as shown in figure 5.7.(e). Knowing α, we can then measure the thickness of a very large number of carbon nanotube films by measuring the extinction.
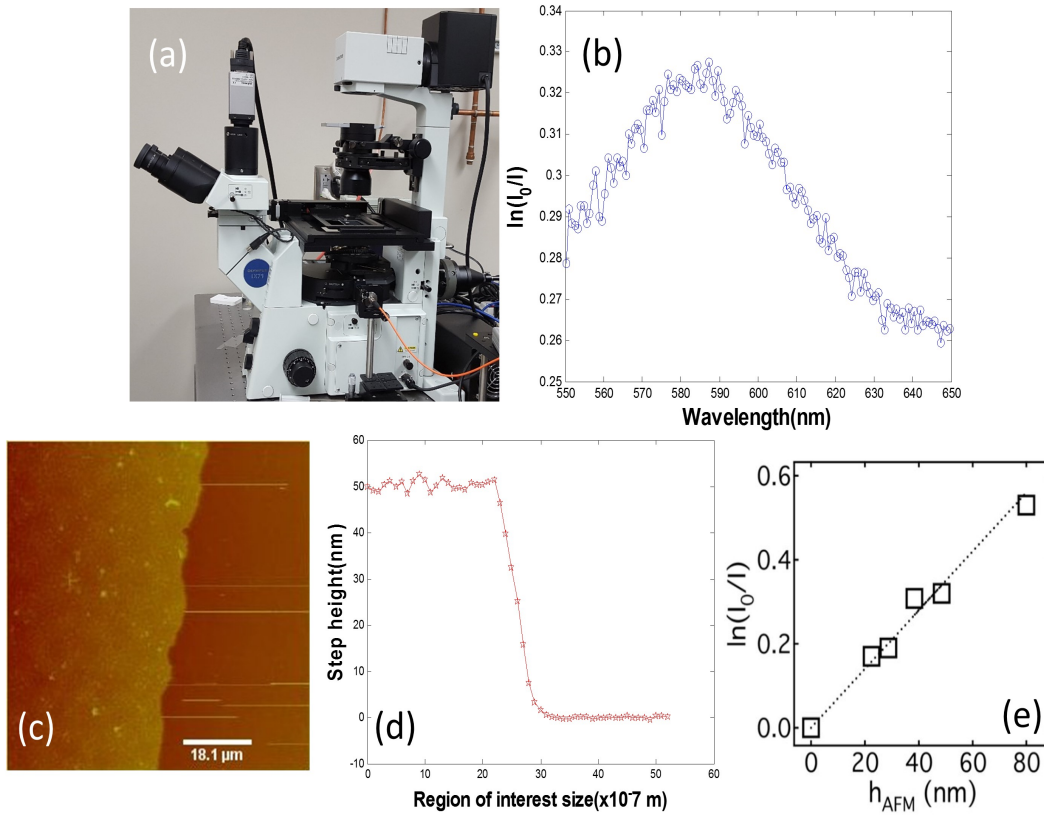
Figure 5.7. (a) The UV-vis spectrometer used to measure the absorption characteristics of the films. (b) Absorption vs. wavelength as measured by the spectrometer. (c) An AFM image of a film deposited on glass. (d) Measured step height from (c). (e) Fitting the absorption peak vs. film thickness to find the extinction coefficent, α.

5.4.3. Other parameters

We also need to find the other parameters contained in equation (5.11). The deformation size, l, and the characteristic length, l_0, were measured from the digital video with the help of 'Image J' software. The width, w, was measured using a Vernier caliper after the films were deposited on the glass substrate. The viscosity of ethanol, μ, was taken from the literature.
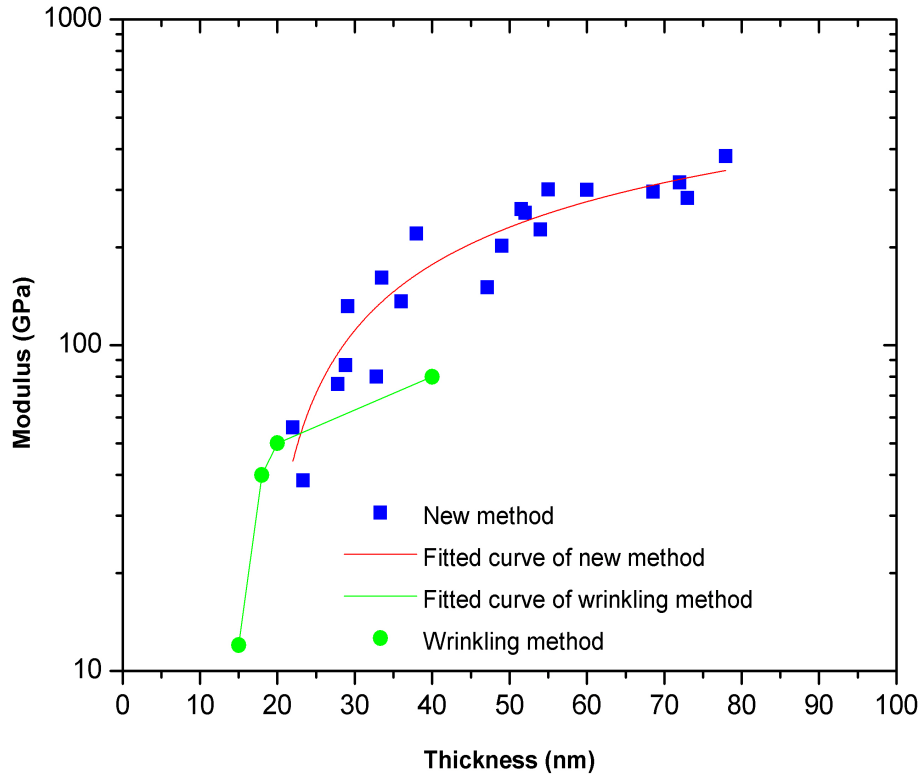
Figure 5.8. Modulus vs. thickness using the new method as compared to the wrinkling method.

5.4.4. Modulus vs. thickness, and comparison

Finally, the modulus of the film was determined based on all of the measured parameters − relaxation time τ, thickness h, deformation size l, characteristic hydrodynamic length l_0, ethanol viscosity μ, and flag width w. A series of films of different thickness were tested (20 nm to 80 nm) and the results are shown in figure 5.8. Although future calibration experiments are planned, our results so far show good agreement with the existing wrinkling method.

5.5. Conclusion

In conclusion, we were able to establish a new fluid-based technique to measure the Young's modulus of thin freestanding SWCNT films, where our approach models the films as an over-damped harmonic oscillator. We find encouraging agreement with independent results obtained on comparable films prepared from the same material using the wrinkling technique. The results demonstrate that at lower film thicknesses close to the percolation threshold, the moduli of the films drops significantly. However, by 50 nm thickness, the modulus of the films starts to level off, signifying an approach to bulk-like behavior. This behavior is somewhat reminiscent of results that have been found for different polymer films based on both experimental [36][39] and theoretical [1] studies. The method is enabled by the striking rigidity of SWCNT thin film. Whereas the wrinkling method provides insight into the extreme conditions typically encountered during applications, our new method mimics the conditions encountered during processing of the films. Additional work focused on calibrating the technique using a material of known modulus and additional work focused on refining the model, as well as simulations of the film relaxation process, are ongoing.

REFERENCES

[1] Zhimin Ao and Sean Li. Temperature- and thickness-dependent elastic moduli of polymer thin films. *Nanoscale Research Letters*, 6(1):243, 2011.

[2] Ray H. Baughman, Anvar A. Zakhidov, and Walt A. de Heer. Carbon nanotubes–the route toward applications. *Science*, 297(5582):787–792, 2002.

[3] A.K. Bhattacharya and W.D. Nix. Analysis of elastic and plastic deformation associated with indentation testing of thin films on substrates. *International Journal of Solids and Structures*, 24(12):1287 – 1298, 1988.

[4] A. P. Bolshakov, S. A. Uglov, A. V. Saveliev, V. I. Konov, A. A. Gorbunov, W. Pompe, and A. Graff. A novel CW laser-powder method of carbon single-wall nanotubes production. *Diamond and Related Materials*, 11:927–930, March 2002.

[5] X. Cai and H. Bangert. Hardness measurements of thin films-determining the critical ratio of depth to thickness using fem. *Thin Solid Films*, 264(1):59 – 71, 1995.

[6] Qing Cao and John A. Rogers. Ultrathin films of single-walled carbon nanotubes for electronics and sensors: A review of fundamental and applied aspects. *Advanced Materials*, 21(1):29–53, 2009.

[7] Moni Kanchan Datta, Jeffrey Maranchi, Sung Jae Chung, Rigved Epur, Karan Kadakia, Prashanth Jampani, and Prashant N. Kumta. Amorphous silicon–carbon based nano-scale thin film anode materials for lithium ion batteries. *Electrochimica Acta*, 56(13):4717 – 4723, 2011.

[8] Z. Fakhraai and J. A. Forrest. Measuring the surface dynamics of glassy polymers. *Science*, 319(5863):600–604, 2008.

[9] T. Guo, P. Nikolaev, A. Thess, D.T. Colbert, and R.E. Smalley. Catalytic growth of single-walled manotubes by laser vaporization. *Chemical Physics Letters*, 243(1):49 – 54, 1995.

[10] M.A. Haque and M.T.A. Saif. Application of {MEMS} force sensors for in situ mechanical characterization of nano-scale thin films in {SEM} and {TEM}. *Sensors and Actuators A: Physical*, 97–98:239 – 245, 2002. Selected papers from Eurosenors {XV}.

[11] John M. Harris, Ji Yeon Huh, Matthew R. Semler, Thomas Ihle, Christopher M. Stafford, Steven D. Hudson, Jeffrey A. Fagan, and Erik K. Hobbie. Elasticity and rigidity percolation in flexible carbon nanotube films on pdms substrates. *Soft Matter*, 9:11568–11575, 2013.

[12] John M. Harris, Ji Yeon Huh, Matthew R. Semler, Thomas Ihle, Christopher M. Stafford, Steven D. Hudson, Jeffrey A. Fagan, and Erik K. Hobbie. Elasticity and rigidity percolation in flexible carbon nanotube films on pdms substrates. *Soft Matter*, 9:11568–11575, 2013.

[13] Z. B. He, Jean-Luc Maurice, C. S. Lee, C. S. Cojocaru, and D. Pribat. Nickel catalyst faceting in plasma-enhanced direct current chemical vapor deposition of carbon nanofibers. *Arabian Journal for Science and Engineering*, 35(1C):19, June 2010. 8 pages.

[14] E. K. Hobbie, D. O. Simien, J. A. Fagan, J. Y. Huh, J. Y. Chung, S. D. Hudson, J. Obrzut, J. F. Douglas, and C. M. Stafford. Wrinkling and strain softening in single-wall carbon nanotube membranes. *Phys. Rev. Lett.*, 104:125505, Mar 2010.

[15] E. K. Hobbie, D. O. Simien, J. A. Fagan, J. Y. Huh, J. Y. Chung, S. D. Hudson, J. Obrzut, J. F. Douglas, and C. M. Stafford. Wrinkling and strain softening in single-wall carbon nanotube membranes. *Phys. Rev. Lett.*, 104:125505, Mar 2010.

[16] Erik K. Hobbie, Thomas Ihle, John M. Harris, and Matthew R. Semler. Empirical evaluation of attractive van der waals potentials for type-purified single-walled carbon nanotubes. *Phys. Rev. B*, 85:245439, Jun 2012.

[17] Sumio Iijima. Helical microtubules of graphitic carbon. *Nature*, 354(6348):56–58, 1991.

[18] Sumio Iijima and Toshinari Ichihashi. Single-shell carbon nanotubes of 1-nm diameter. *Nature*, 363(6430):603–605, 1993.

[19] Tomoaki Ikegami, Futoshi Nakanishi, Makoto Uchiyama, and Kenji Ebihara. Optical measurement in carbon nanotubes formation by pulsed laser ablation. *Thin Solid Films*, 457(1):7 – 11, 2004. The 16th Symposium on Plasma Science for Materials (SPSM-16).

[20] Y. Jiang, H. Wang, X. F. Shang, Z. H. Li, and M. Wang. Influence of nh3 atmosphere on the growth and structures of carbon nanotubes synthesized by the arc-discharge method. *Inorganic Materials*, 45(11):1237, 2009.

[21] W. Kratschmer, Lowell D. Lamb, K. Fostiropoulos, and Donald R. Huffman. Solid c60: a new form of carbon. *Nature*, 347(6291):354–358, 1990.

[22] Ivar Kruusenberg, Nadezda Alexeyeva, Kaido Tammeveski, Jekaterina Kozlova, Leonard Matisen, Väino Sammelselg, Jose Solla-Gullón, and Juan M. Feliu. Effect of purification of carbon nanotubes on their electrocatalytic properties for oxygen reduction in acid solution. *Carbon*, 49(12):4031 – 4039, 2011.

[23] Qianqian Li, Michael Zaiser, Jane R. Blackford, Chris Jeffree, Yehong He, and Vasileios Koutsos. Mechanical properties and microstructure of single-wall carbon nanotube/elastomeric epoxy composites with block copolymers. *Materials Letters*, 125:116 – 119, 2014.

[24] Chung-Jen Lu and D.B. Bogy. The effect of tip radius on nano-indentation hardness tests. *International Journal of Solids and Structures*, 32(12):1759 – 1770, 1995.

[25] R. Marchiori, W. F. Braga, M. B. H. Mantelli, and A. Lago. Analytical solution to predict laser ablation rate in a graphitic target. *Journal of Materials Science*, 45(6):1495–1502, 2010.

[26] P. A. O'Connell and G. B. McKenna. Rheological measurements of the thermoviscoelastic response of ultrathin polymer films. *Science*, 307(5716):1760–1763, 2005.

[27] Jan Prasek, Jana Drbohlavova, Jana Chomoucka, Jaromir Hubalek, Ondrej Jasek, Vojtech Adam, and Rene Kizek. Methods for carbon nanotubes synthesis-review. *J. Mater. Chem.*, 21:15872–15884, 2011.

[28] H.J. Qi, K.B.K. Teo, K.K.S. Lau, M.C. Boyce, W.I. Milne, J. Robertson, and K.K. Gleason. Determination of mechanical properties of carbon nanotubes and vertically aligned carbon nanotube forests using nanoindentation. *Journal of the Mechanics and Physics of Solids*, 51(11–12):2213 – 2237, 2003. Proceedings of a Symposium on Dynamic Failure and Thin Film Mechanics, honoring Professor L.B. Freund.

[29] Ranjana Saha and William D. Nix. Effects of the substrate on the determination of thin film mechanical properties by nanoindentation. *Acta Materialia*, 50(1):23 – 38, 2002.

[30] R. Saito, M. Fujita, G. Dresselhaus, and M. S Dresselhaus. Electronic structure of chiral graphene tubules. *Applied Physics Letters*, 60(18):2204–2206, 1992.

[31] R. (Riichiro) Saito, M. S Dresselhaus, and G Dresselhaus. *Physical properties of carbon nanotubes.* London : Imperial College Press, 1998. Includes bibliographical references (p.239-251) and index.

[32] Matthew R. Semler, John M. Harris, Andrew B. Croll, and Erik K. Hobbie. Localization and length-scale doubling in disordered films on soft substrates. *Phys. Rev. E*, 88:032409, Sep 2013.

[33] Matthew R. Semler, John M. Harris, Andrew B. Croll, and Erik K. Hobbie. Localization and length-scale doubling in disordered films on soft substrates. *Phys. Rev. E*, 88:032409, Sep 2013.

[34] R.S. Singh, V.K. Rangari, S. Sanagapalli, V. Jayaraman, S. Mahendra, and V.P. Singh. Nanostructured cdte, cds and tio2 for thin film solar cell applications. *Solar Energy Materials and Solar Cells*, 82(1–2):315 – 330, 2004. {CANCUN} 2003.

[35] Christopher M. Stafford, Christopher Harrison, Kathryn L. Beers, Alamgir Karim, Eric J. Amis, Mark R. VanLandingham, Ho-Cheol Kim, Willi Volksen, Robert D. Miller, and Eva E. Simonyi. A buckling-based metrology for measuring the elastic moduli of polymeric thin films. *Nature*, 3(8):545–550, 2004.

[36] Christopher M. Stafford, Bryan D. Vogt, Christopher Harrison, Duangrut Julthongpiput, and Rui Huang. Elastic moduli of ultrathin amorphous polymer films. *Macromolecules*, 39(15):5095–5099, 2006.

[37] Stephen A. Steiner, Theodore F. Baumann, Bernhard C. Bayer, Raoul Blume, Marcus A. Worsley, Warren J. MoberlyChan, Elisabeth L. Shaw, Robert Schlögl, A. John Hart, Stephan Hofmann, and Brian L. Wardle. Nanoscale zirconia as a nonmetallic catalyst for graphitization of carbon and growth of single- and multiwall carbon nanotubes. *Journal of the American Chemical Society*, 131(34):12144–12154, 2009. PMID: 19663436.

[38] Jeong-Yun Sun, Shuman Xia, Myoung-Woon Moon, Kyu Hwan Oh, and Kyung-Suk Kim. Folding wrinkles of a thin stiff layer on a soft substrate. *Proceedings of the Royal Society of London A: Mathematical, Physical and Engineering Sciences*, 2011.

[39] Jessica M. Torres, Christopher M. Stafford, and Bryan D. Vogt. Elastic modulus of amorphous polymer thin films: Relationship to the glass transition temperature. *ACS Nano*, 3(9):2677–2685, 2009. PMID: 19702280.

[40] Zhi-Hui Xu and David Rowcliffe. Finite element analysis of substrate effects on indentation behaviour of thin films. *Thin Solid Films*, 447–448:399 – 405, 2004. Proceedings of the 30th International Conference on Metallurgical Coatings and Thin Films.

[41] Wei Xue and Tianhong Cui. Characterization of layer-by-layer self-assembled carbon nanotube multilayer thin films. *Nanotechnology*, 18(14):145709, 2007.

[42] Zhaohui Yang, Yoshihisa Fujii, Fuk Kay Lee, Chi-Hang Lam, and Ophelia K. C. Tsui. Glass transition dynamics and surface layer mobility in unentangled polystyrene films. *Science*, 328(5986):1676–1679, 2010.

[43] Yanjuan Zhu, Tianjin Lin, Qiuxiang Liu, Yulian Chen, Guofu Zhang, Huifang Xiong, and Haiyan Zhang. The effect of nickel content of composite catalysts synthesized by hydrothermal method on the preparation of carbon nanotubes. *Materials Science and Engineering: B*, 127(2–3):198 – 202, 2006.

APPENDIX. MATLAB CODE TO EXTRACT THE RELAXATION TIME

```
%%Extracting & Saving of frames from a Video file through Matlab Code%%
clc;
close all;
clear all;
%{
% assigning the name of sample avi file to a variable
filename = '20170223rebound60nmmnprev1okk.avi';


%reading a video file
mov = VideoReader(filename);


% Defining Output folder as 'snaps'
opFolder = fullfile(cd, 'snaps');
%if not existing
if ~exist(opFolder, 'dir')
%make directory & execute as indicated in opfolder variable
mkdir(opFolder);
end


%getting no of frames
numFrames = mov.NumberOfFrames;


%setting current status of number of frames written to zero
numFramesWritten = 0;
```

```matlab
%for loop to traverse & process from frame '1' to 'last' frames
for t = 1 : numFrames
currFrame = read(mov, t);      %reading individual frames
opBaseFileName = sprintf('%3.3d.png', t);
opFullFileName = fullfile(opFolder, opBaseFileName);
imwrite(currFrame, opFullFileName, 'png');     %saving as 'png' file
%indicating the current progress of the file/frame written
progIndication = sprintf('Wrote frame %4d of %d.', t, numFrames);
disp(progIndication);
numFramesWritten = numFramesWritten + 1;
end        %end of 'for' loop
progIndication =
sprintf('Wrote %d frames to folder "%s"',numFramesWritten, opFolder);
disp(progIndication);
%End of the code
%}
%%Extracting Excel files from the frames%%
for tt=1:600


    sm=10;
filenamee = sprintf('%3.3d.png', tt);
data = imread(filenamee);
 % I2 = imcrop(data1,[75 68 130 112]);
  % J = imnoise(data1,'gaussian',0,0.1);
  %imshow(data1);
  %data1=imrotate(data,-10);
  BW = im2bw(data, 0.32);
 % BW= ~BW;
```

```matlab
% BW2= bwareaopen(BW,20);


%I = bwperim(BW);
BW3 = bwmorph(BW,'thin',Inf);
I=BW3;
%I= bwareaopen(BW3,20);



%s = regionprops(BW2,'Perimeter');
%p=s(1).FilledImage;
%BW4 = bwmorph(p,'thin',Inf);


[x,y]=find(I==1);
figure
%plot(centroids(:,1),centroids(:,2), 'b*')
imshow(I);
dl=0;
dk=0;
for i=1:length(x)
if i==1
        s=0;
    end

    if i~=1
        ds = (x(i)-x(i-1))^2 + (y(i)-y(i-1))^2;
        dk=sqrt(ds);
        s(i)=dk+dl;
        dl=s(i);
    end
```

```matlab
end


sum = 500;
c = 1;
match = 0;
dl=0;
dk=0;
for i= 1:length (x)
    p(i) = x(c); q(i) = y(c);


     if i==1
         s=0;
    end


    if i~=1
        ds = (p(i)-p(i-1))^2 + (q(i)-q(i-1))^2;
        dk=sqrt(ds);
        s(i)=dk+dl;
        dl=s(i);
    end
     if i~=1 && p(i-1)==p(i)&& q(i-1)==q(i)
     break
     end


    for l=length(x):-1:1
      %{
       l=c+l11;
```

```matlab
 if  l>length(x)
      l=c+l11-length(x);
 end
%}
for  j = 1:length(x)
    match = 0;
  for  jj = 1:length(p)
      %/if  j<= jj
      if  x(l) == p(jj) && y(l) == q(jj)
          match = 1;
          break;
      end
  end


    %/ end
    if  match == 0
      if  rem(l,2) == 1
          if  ((x(l)-x(c))^2 + (y(l)-y(c))^2) < sum
              sum = (x(l)-x(c))^2 + (y(l)-y(c))^2;
              dd=0; n=l;
          end
      end
      if  rem(l,2) == 0
          if  ((x(l)-x(c))^2 + (y(l)-y(c))^2) < sum
              sum = (x(l)-x(c))^2 + (y(l)-y(c))^2;
              dd=1; m=l;
          end
      end
    end
```

```matlab
            end
        end




                if dd == 0
                    c = n;
                    sum = 5000;
                end
                if dd == 1
                    c = m;
                    sum = 5000;
                end
    end



mp = 30; mq =40;


ls=length(s);
if rem(ls,2)==0
    lp1=ls/2;
end
if rem(ls,2)~=0
    lp1=(ls-1)/2;
end
```

```matlab
prv=0;


xs=zeros(1,lp1);
ys=zeros(1,lp1);
s12=zeros(1,lp1);
for  i3=1:lp1
  xs(i3)=p(i3);
  ys(i3)=q(i3);
  s12(i3)=s(i3);

  dist=(xs(i3)-mp)^2+(ys(i3)-mq)^2;
  tldist=prv+dist;
  prv=tldist;
end




prv11=0;

lp2=lp1;
xs11=zeros(1,ls-lp2);
ys11=zeros(1,ls-lp2);
s211=zeros(1,ls-lp2);
s111=zeros(1,ls-lp2);
```

```matlab
for i3 =1: ls −lp2
 xs11 ( i3 )=p( lp2+i3 ) ;
 ys11 ( i3 )=q( lp2+i3 ) ;
 s211 ( i3 )=s ( i3 ) ;
 dist11 =(xs11 ( i3 )−mp)^2+(ys11 ( i3 )−mq)^2 ;
 tldist11=prv11+dist11 ;
 prv11=tldist11 ;
end

if tldist >tldist11
r=xs ;
c=ys ;
s1=s12 ;
end
if tldist11 >tldist
r = fliplr ( xs11 ) ;
c= fliplr ( ys11 ) ;
bb=0;
kk=0;
for i5 =1: ls −lp2
    if i5==1
     s1 =0;
    end
    if i5 >1

    vv=s ( ls −bb)− s ( ls −bb−1);
    bb=bb+1;
    s1 ( i5 )=vv+kk ;
    kk=s1 ( i5 ) ;
```

```matlab
        end
    end


    end



BW4 = bwselect(I,c,r,1);
figure
imshow(BW4)



pp=p;
qq=q;
ss=s1;

%}
pp=x;
qq=y;
ss=s;



lp=length(pp);


fz=0;


for  i1=1:length(ss)
```

```matlab
if i1>sm && i1<=lp-sm
    fz=fz+1;
    cp(fz)=pp(i1);
    cq(fz)=qq(i1);
    cs(fz)=ss(i1);
    for j1=1:2*sm+1
    pc1(j1)=pp(i1+j1-sm-1);
    qc1(j1)=qq(i1+j1-sm-1);
    sc1(j1)=ss(i1+j1-sm-1);
    end
    pc2=pc1';
    qc2=qc1';
    sc2=sc1';
f1=fit(sc2,pc2,'poly2');
f2=fit(sc2,qc2,'poly2');


k1=f1.p1;
k2=f2.p1;


curvature(fz)=2*sqrt(k1*k1+k2*k2);
end



end

xs1=cp';
ys1=cq';
ss1=cs';
curvaturee=curvature';
```

```matlab
matrix=[xs1 ys1 ss1 curvaturee];


filename = sprintf('e%3.3d.xlsx', tt);
xlswrite(filename,matrix);


clc
clear all;
close all;


end
%}


%%Finding the minimum length of vectors among all the excel files%%
t=0;
d=5000;
c=0;
dd=0;
for i=1:600
    t=t+1;
    filename=sprintf('e%3.3d',i);
    a=xlsread(filename);
    if rem(t,2)~=0
        m=length(a);


    else
        n=length(a);
    end
    if t~=1
        if length(a)<50
```

```
            dd=dd+1;

            kk(dd)=i;

        end


        if m<d

            c=t;

          d=m;

          end
        if n<d

            c=t;

            d=n;

        end


    end
    end
%}


%%Creating an excel file composed of all the normalized curvature data%%
b=[];
for i=1:600
    filename=sprintf('e%3.3d',i);
    a=xlsread(filename);
     if length(a)> 49
     b=[b a(1:50,4)];
      end
end
xlswrite('new.xlsx',b);


    %}
```

```
%%Exponential model fitting to the data%%
clc
close all;
clear all;
filename = 'data1.xlsx';
p= xlsread(filename,'A:A');
q = xlsread(filename,'B:B');
d=0;
ft=fittype('a*exp(-(b*x))+c','coefficients',{'a','b','c'});
f=fit(p,q,ft);
k=f.b;
%k1=f.c;
fdata = feval(f,p);
I = abs(fdata - q) > 0.2*std(q);
outliers = excludedata(p,q,'indices',I);


fit2 = fit(p,q,ft,'Exclude',outliers);


%subplot(1, 2, 1);
%plot(f,p,q);



fit3 = fit(p,q,ft,'robust','on');
realk=fit3.b;
%realk1=fit3.n;


%subplot(1, 2, 2);
plot(fit3,p(~outliers),q(~outliers),'k.')
xlabel('time (s)','fontweight','bold','fontsize',16);
```

```
ylabel('Curvature (1/\mum)','fontweight','bold','fontsize',16);
%hold on

xx=p(~outliers);
yy=q(~outliers);
%plot(fit2,'c--')
%plot(fit3,'b:')


%}
```